Stem Cell Reports, Volume *7*

Supplemental Information

Development and Dynamic Regulation of Mitochondrial Network in Human Midbrain Dopaminergic Neurons Differentiated from iPSCs

Du Fang, Yu Qing, Shijun Yan, Doris Chen, and Shirley ShiDu Yan

Supplemental Information

Development and Dynamic Regulation of Mitochondrial Network in Human Midbrain Dopaminergic Neurons Differentiated from iPSC

Du Fang[1,3], Yu Qing [1,2,3], Shijun Yan[1], Doris Chen[1], Shirley ShiDu Yan[1]*

Supplemental Figures and Legends

Supplementary Figure S1.

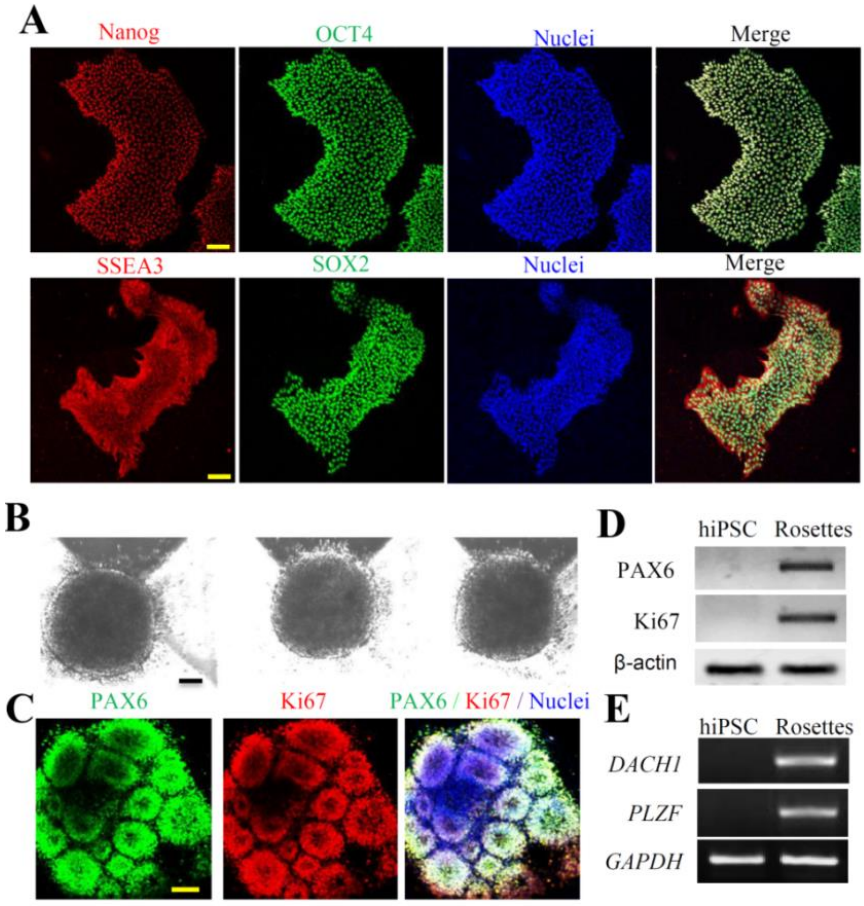

Figure S1 (Related to results: hiPSC characterization and DA neuron-directed differentiation). Characterization and identification of hiPSC line derived from normal human bone marrow fibroblasts. (S1A).

Normal human bone marrow fibroblast-derived hiPSCs BM2-3 was selected for analysis. hiPSC-BM2-3 cells expressed pluripotency markers: NANOG, OCT4, SSEA3 and SOX2. (**S1B**) Formation of embryonic bodies (EB), neural aggregates and (**S1C**) rosettes (lower panel) of hiPSC-BM2-3 cells. Images in the top panel show EB formation after forced aggregation of

hiPSC-BM2-3 cells using Aggrewells. Images in the bottom panel show rosette formations with rosette-like structures co-expressing early-stage precursor cells marker PAX6 (Green) and the mitotic marker Ki67 (Red). Nuclei were stained by DRAQ5 (5 μM, Cell Signaling), a far-red emitting fluorescent DNA dye, for 3 min at room temperature. Scale bars, 50 μm. (**S1D**) immunoblotting analysis to detect PAX6 and Ki67 and (**S1E**), semi-quantitative RT-PCR analysis to observe expression of "rosette-specific" genes of *DACH1* and *PLZF*, while no expressions were detected in hiPSC cells.

Supplementary Figure S2.

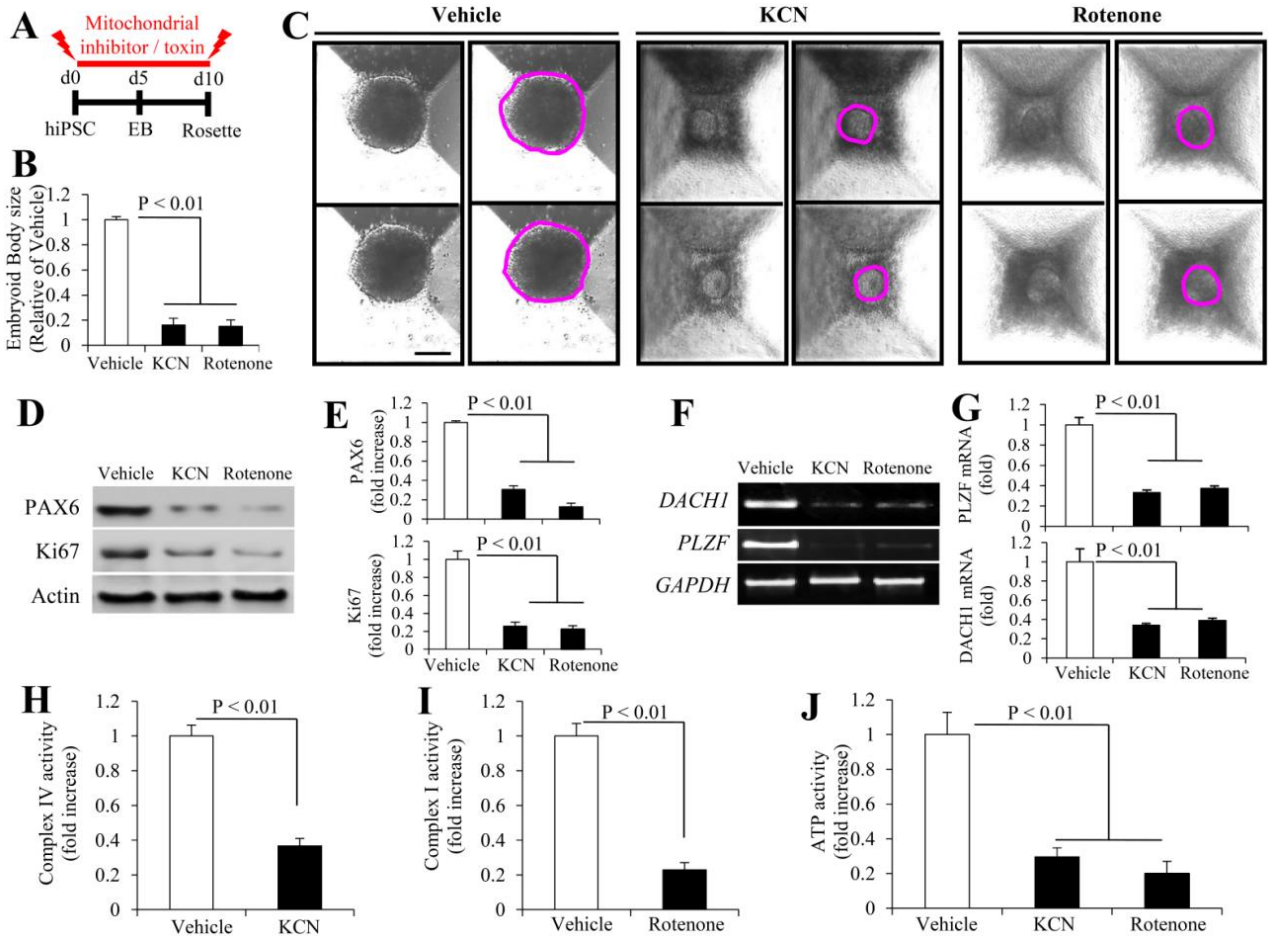

Figure S2 (Related to results: Effect of mitochondrial function on DA neuron-directed differentiation). Effects of KCN and rotenone on EB and rosette formations.

(**S2A**) A schematic representation of the neural EB and rosette formations under KCN or rotenone treatments. (**S2B**) Quantification of EB morphology shown in **S2C** (n = 3 independent experiments; mean ± SEM. 10 EBs in each group were traced per experiment). (**S2D-E**) immunoblotting analysis to detect PAX6 and Ki67. Representative immunoblots for PAX6, Ki67 and β-actin. Data are expressed as fold increase relative to vehicle rosette (**S2E**). β-actin was used as a protein loading control (n = 3 independent experiments; mean ± SEM). (**S2F-G**), semi-

quantitative RT-PCR analysis to observe expression of "rosette-specific" genes of *DACH1* and *PLZF*. Representative semi-quantitative RT-PCR images for *DACH1*, *PLZF* and *GAPDH* (**S2F**). Data are expressed as fold increase relative to vehicle rosette (**S2G**). *GAPDH* was used as a control (n = 3 independent experiments; mean ± SEM). Enzymatic activity of complex IV (**H**), I (**I**), and cellular ATP levels (**J**) were determined in cell lysates from rosette with or without KCN and rotenone treatments. Data are expressed as fold increase relative to vehicle rosette (n = 3 independent experiments; mean ± SEM). Scale bar, 200µm. Statistical analysis was performed using Statview software (SAS Institute, Version 5.0.1). For **B**, **E, G** and **J**, one-way ANOVA was used for repeated measure analysis, followed by Fisher's protected least significant difference for post hoc comparisons. Student's *t* test was used for **H** and **I**.

Supplementary Video S1. (Related to figure 4E-J and figure 6M-R). Mitochondrial movement in the neurites of hiPSC-derived DA neurons with different treatments.

Videos S1A-C: mitochondrial movement in the neurites of hiPSC-derived DA neurons differentiated for 10 days (**Video S1A)**; 15 days (**Video S1B**) and 20 days (**Video S1C**). In the neuronal process of hiPSC-derived DA neurons differentiated for 15 (**Video S1B**) and 20 days (**Video S1C**), mitochondria showed elongated morphology and movement with significantly higher speed and longer travel distance. **Videos S1D-F**: mitochondrial movement in the neurites of hiPSC-derived DA neurons differentiated for 20 days (**Video S1D**) with or without KCN (**Video S1E**) or rotenone (**Video S1F**) treatments, mitochondria showed shortened morphology and significantly less movement.

Supplemental Experimental Procedures

Immunoblotting analysis

Differentiated cells cultured in DA neuronal differentiation medium for 5, 10, 15 and 20 days or the rosettes were washed with ice-cold PBS and proteins extracted with 150μl of lysis buffer. After centrifugation at 12,000 × g for 10 min at 4°C, we collected the supernatant and determined protein concentrations; we boiled 30 μg proteins in protein loading buffer for 5 min, separated the proteins on a 10% SDS polyacrylamide gel, and subsequently transferred to nitrocellulose membranes. Nonspecific binding was inhibited by incubation in TBST (20 mM Tris-buffered saline with 0.1% Tween 20, pH 7.5) containing 5% nonfat dried milk for 1 hour at room temperature. Membranes were incubated with the following primary antibodies: Rabbit anti-PAX6 (1:1000, 42-6600, Invitrogen), mouse anti-Ki67 (1:1000, 556003, BD Pharmingen™), Rabbit anti-Oct-4 (Octamer-binding transcription factor 4, 1:1000, Life Technologies), Rabbit anti-TH (tyrosine hydroxylase, 1:2000, Chemicon, Temecula, CA), mouse anti-TuJ1 (class III β-tubulin, 1:10000, Sigma), and rabbit anti-syn (synaptophysin, 1:5000, A0010, Dako) overnight at 4°C. After three washes with TBST, membranes were incubated for 2 h with horseradish (HRP)-conjugated secondary antibodies (Pierce Chemical Company, USA) and developed using enhanced chemiluminescence (ECL Amersham Biosciences, England). To ensure equal protein loading of the samples, the same membrane was probed with anti-mouse β-actin monoclonal antibody (Sigma-Aldrich, MO) at a 1:10,000 dilution.

Immunocytochemistry

The BM2-3 hiPSCs, at 16 passages, the induced DA neurons, after differentiation for 5, 10, 15 and 20 days, or the attached neural aggregates, all cultured on coverslips, were fixed with 4% ice-cold paraformaldehyde for 5 min and then permeabilized with PBS containing 0.1% Triton

and 5% goat serum for 1 h followed by incubation with the following primary antibodies: rabbit anti-Oct4 (1:2500, A13998, Life Technologies) and mouse anti-Nanog (1:2500, ab173368, abcam); rabbit anti-SOX2 (1:2500, A13992; Life Technologies) and rat anti-SSEA3 (1:500, 41-4400, Life Technologies); Rabbit anti-PAX6 (1:1000, 42-6600, Invitrogen) and mouse anti-Ki67 (1:1000, 556003, BD Pharmingen™); rabbit anti-TH (1:2000, Chemicon, Temecula, CA) and mouse anti-TuJ1 (1:10000, Sigma), or rabbit anti-TH (1:2000, Chemicon, Temecula, CA) and mouse anti-Syn IgG (1:1000, chemicon) at 4°C for 16 h. Cells were incubated with Alexa Fluor 488-conjugated goat anti-rabbit IgG and 594 goat anti-mouse/rat IgG (1: 1000, Invitrogen) or Alexa Fluor 594-conjugated goat anti-rabbit IgG and 488 goat anti-mouse IgG (1: 1000, Invitrogen) for 1 h at room temperature. After washing with PBS, neurons were covered with Vectashield mounting medium (H-1000, Vector Laboratories). Images were acquired (equal exposure for all groups) using confocal microscopy (Leica) and analyzed using the Universal Metamorph Image Program.

We measured synaptic density of cultured neurons by counting the number of synaptophysin-positive clusters in neuronal dendrites and puncta per 100 microns of TH positive dendrite (presented as the number of synaptophysin clusters per 100 microns of dendrite) and calculated by dividing the length of the TH+ dendrites.

Real-time PCR measurement

RNA was extracted identified cells by using TRIzol reagents (Invitrogen, Carlsbad, CA, USA) according to the manufacturer's protocol as described in our previous study (Fang et al., 2015). cDNA was directly proformed using TaqMan reverse transcription reagents kit (Applied Biosystems, Foster City, CA, USA). Total RNA (1 μg) was used for the synthesis of cDNA with TaqMan Reverse Transcription Reagents kit (Roche Applied Biosystems). Real time-PCR was

performed on an ABI Prism 7900 Sequence Detection System (Applied Biosystems) with TaqMan PCR Master Mix. Semi-quantitative PCR was performed in the GeneAmp PCR System 2720 (Applied Biosystems), and same volume of reaction products are electrophoresed on an agarose gel. The sequences of the primers were EN1 (Hs00154977_m1, Thermo Fisher), OTX2 (Hs00222238_m1, Thermo Fisher), FOXA2 (Hs00232764_m1, Thermo Fisher), map2 (Hs00258900_m1, Thermo Fisher), DDC (AADC) (Hs01105048_m1, Thermo Fisher), SLC18A2 (VMAT2) (Hs00996835_m1, Thermo Fisher), LMX1A (Hs00892663_m1, Thermo Fisher), SLC6A3 (DAT) (Hs00997374_m1, Thermo Fisher), ZBTB16 (PLzf) (Hs00957433_m1, Thermo Fisher), DACH1 (Hs00362088_m1, Thermo Fisher).

Electrophysiology analysis

Electrophysiologic experiments were performed on day-10, -15 and -20 differentiated DA neurons. Electrophysiology recordings were performed as described previously (Vierbuchen et al., 2010). We analyzed cells at indicated times after induction, recording resting membrane potential as well as spontaneous and evoked action potentials using current clamp whole-cell configuration. Evoked action potentials were recorded at a holding potential on resting membrane potential; step currents ranging from -10 pA to +90 pA were injected at 20 pA to elicit action potentials. Whole-cell currents including sodium currents and potassium currents were recorded at a holding potential of -70 mV, with voltage steps ranging from -70 mV to +50 mV delivered at 10 mV increments. Spontaneous postsynaptic currents (sPSCs) were recorded at a holding potential of -70 mV with voltage clamp configuration. The pipette solution for patch-clamp experiments contained (in mM) 130 K-gluconate, 10 KCl, 5 $MgCl_2$, 5 HEPES, 0.6 EGTA, 0.06 $CaCl_2$, 2 MgATP, and 0.2 Na_2GTP, pH adjusted to 7.2 with KOH. The recording bath solution contained (in mM) 119 NaCl, 5 KCl, 20 HEPES, 30 glucose, 2 $CaCl_2$ and 2 $MgCl_2$, pH

adjusted to 7.3 with NaOH. We acquired whole-cell patch clamp recordings using a MultiClamp 700B amplifier, Digidata 1440A, and Clampex data acquisition software (Molecular Devices) at room temperature.

Measurement of respiratory chain complex enzyme activities and ATP levels

Enzyme activities in complex I (NADH-ubiquinonereductase), complex IV (cytochrome c oxidase, CcO), and ATP levels were determined as described previously (Gan et al., 2014a). The reaction was then initiated by the addition of 50 µl of ferrocytochrome substrate solution (0.22 mM) and changes in absorbance of cytochrome c at 550 nm were measured using a Shimadzu (Kyoto, Japan) UV1200 spectrophotometer. Activity is expressed as micromoles of cytochrome oxidized per min^{-1} mg^{-1} protein using an extinction coefficient of 18.64 mM^{-1} cm^{-1}.

ATP levels were determined using an ATP Bioluminescence Assay Kit (Roche) following the manufacturer's instructions (Du et al., 2008; Du et al., 2010). Briefly, cells were harvested using the provided lysis buffer, incubated on ice for 15 minutes, and centrifuged at 13,000g for 10 minutes. ATP levels were measured using a Luminescence plate reader (Molecular Devices) with an integration time of 10 seconds.

Determination of mitochondrial membrane potential (ΔΨ) with TMRM and Mitochondrial ROS generation with Mitosox Red

Differentiated neuronal cells were seeded at low density onto Lab-Tek eight-well chamber slides (10,000 cells /well). Mitochondrial ROS generation was determined using MitoSox Red (Invitrogen), a unique fluorogenic dye highly selective for detection of superoxide production in live cell mitochondria (Gan et al., 2014a; Gan et al., 2014b; Iuso et al., 2006; Polster et al., 2014; Xu and Chisholm, 2014). Cells were incubated with fresh medium containing 2.5 µM MitoSox for 30 min at 37°C. To detect mitochondrial membrane potential, cells were co-stained with

TMRM (100nM; Invitrogen) for 30 min and MitoTracker Green (MTGreen, 100nM, Invitrogen). In addition, mitochondria were labeled with Mitotracker Red (MTRed, 100nM, Invitrogen) for 30 min at 37 °C before fixation to visualize morphology. Fluorescence images were acquired on a Leica SP5 confocal microscope and analyzed using Leica LAS AF software (Leica Wetzlar). Excitation wavelengths were 543 nm for MitoSox, TMRM or MTRed, and 488nm for MTGreen, respectively. Fluorescent signals were quantified using NIH Image J software. We used MetaMorph (Molecular Devices) and NIH Image J software for quantification and measurement of fluorescent signals of mitochondrial length and mitochondrial density. Mitochondrial size, shape, density, and fluorescent intensity were quantified by an investigator blinded to experimental groups. Mitochondria from 20-25 randomly selected cells were measured and quantified.

Evaluation of intracellular ROS levels

Intracellular ROS levels were accessed by election paramagnetic resonance (EPR) spectroscopy as described in our previous study (Fang et al., 2015; Fang et al., 2016). CMH (cyclic hydroxylamine 1-hydroxy-3-methoxycarbonyl-2, 2, 5, 5-tetramethyl-pyrrolidine, 100μM) was incubated with cultured cells for 30 min and then washed with cold PBS. The cells were collected and homogenized with 100 μl of PBS for EPR measurement. The EPR spectra were collected, stored, and analyzed with a Bruker EleXsys 540 x-band EPR spectrometer (Billerica, MA) using the Bruker Software Xepr (Billerica, MA).

Axonal mitochondrial trafficking recording and data analysis in differentiated neuronal cells

These recordings were performed using previously reported protocols (Du et al., 2010; Guo et al., 2013). Axonal mitochondria were visualized following transfection with pDsRed2-mito (Clontech) in differentiated neuronal cells using lipofectamine LTX and plus regent (Invitrogen)

according to the manufacturer's protocol. Three to four days after transfection, time-lapse recordings of labeled mitochondrial movement were acquired on a Carl Zeiss (Axiovert 200) microscope with incubation system (PeCon) to maintain differentiated neuronal cells at 37°C during image collection. Collection of image stacks and velocity measurements were made using the AxioVision Software as previously described (Du et al., 2010; Guo et al., 2013). For standard recordings, images of mitochondria in one process per differentiated neuronal cell were collected every 3 s for 2 min. Only the proximal segment of the axon was acquired and recorded.

Mitochondria in each frame of every video recording were individually tracked using AxioVision Software and the average velocity was calculated during the 2-min recording period. The average velocity of every mitochondrion in one measured process in each cell was then averaged to obtain the average velocity for mitochondrial movement per process. In addition, the percentage of movable mitochondria, mitochondrial total traveling distance (total distance traveled irrespective of direction during the recording period), single mitochondrial length and mitochondrial density in each process were all determined according to previous studies with modifications (Gan et al., 2014a; Trimmer and Borland, 2005). Exposure periods (30–50 ms) were kept at a minimum to limit phototoxicity.

Statistical analysis

Statistical analysis was performed using Statview software (SAS Institute, Version 5.0.1). One-way ANOVA or Student's *t* test was used for repeated measure analysis, followed by Fisher's protected least significant difference for post hoc comparisons. Data are presented as mean ± SEM. $P < 0.05$ was considered significant.

Supplemental References

Du, H., Guo, L., Fang, F., Chen, D., Sosunov, A.A., McKhann, G.M., Yan, Y., Wang, C., Zhang, H., Molkentin, J.D., *et al.* (2008). Cyclophilin D deficiency attenuates mitochondrial and neuronal perturbation and ameliorates learning and memory in Alzheimer's disease. Nature medicine *14*, 1097-1105.

Du, H., Guo, L., Yan, S., Sosunov, A.A., McKhann, G.M., and Yan, S.S. (2010). Early deficits in synaptic mitochondria in an Alzheimer's disease mouse model. Proceedings of the National Academy of Sciences of the United States of America *107*, 18670-18675.

Fang, D., Wang, Y., Zhang, Z., Du, H., Yan, S., Sun, Q., Zhong, C., Wu, L., Vangavaragu, J.R., Yan, S., *et al.* (2015). Increased neuronal PreP activity reduces Abeta accumulation, attenuates neuroinflammation and improves mitochondrial and synaptic function in Alzheimer disease's mouse model. Human molecular genetics *24*, 5198-5210.

Fang, D., Zhang, Z., Li, H., Yu, Q., Douglas, J.T., Bratasz, A., Kuppusamy, P., and Yan, S.S. (2016). Increased Electron Paramagnetic Resonance Signal Correlates with Mitochondrial Dysfunction and Oxidative Stress in an Alzheimer's disease Mouse Brain. Journal of Alzheimer's disease : JAD *51*, 571-580.

Gan, X., Huang, S., Wu, L., Wang, Y., Hu, G., Li, G., Zhang, H., Yu, H., Swerdlow, R.H., Chen, J.X., *et al.* (2014a). Inhibition of ERK-DLP1 signaling and mitochondrial division alleviates mitochondrial dysfunction in Alzheimer's disease cybrid cell. Biochim Biophys Acta *1842*, 220-231.

Gan, X., Wu, L., Huang, S., Zhong, C., Shi, H., Li, G., Yu, H., Howard Swerdlow, R., Xi Chen, J., and Yan, S.S. (2014b). Oxidative stress-mediated activation of extracellular signal-regulated kinase contributes to mild cognitive impairment-related mitochondrial dysfunction. Free radical biology & medicine *75*, 230-240.

Guo, L., Du, H., Yan, S., Wu, X., McKhann, G.M., Chen, J.X., and Yan, S.S. (2013). Cyclophilin D deficiency rescues axonal mitochondrial transport in Alzheimer's neurons. PloS one *8*, e54914.

Iuso, A., Scacco, S., Piccoli, C., Bellomo, F., Petruzzella, V., Trentadue, R., Minuto, M., Ripoli, M., Capitanio, N., Zeviani, M., *et al.* (2006). Dysfunctions of cellular oxidative metabolism in patients with mutations in the NDUFS1 and NDUFS4 genes of complex I. The Journal of biological chemistry *281*, 10374-10380.

Polster, B.M., Nicholls, D.G., Ge, S.X., and Roelofs, B.A. (2014). Use of potentiometric fluorophores in the measurement of mitochondrial reactive oxygen species. Methods in enzymology *547*, 225-250.

Trimmer, P.A., and Borland, M.K. (2005). Differentiated Alzheimer's disease transmitochondrial cybrid cell lines exhibit reduced organelle movement. Antioxidants & redox signaling *7*, 1101-1109.

Vierbuchen, T., Ostermeier, A., Pang, Z.P., Kokubu, Y., Sudhof, T.C., and Wernig, M. (2010). Direct conversion of fibroblasts to functional neurons by defined factors. Nature *463*, 1035-1041.

Xu, S., and Chisholm, A.D. (2014). C. elegans epidermal wounding induces a mitochondrial ROS burst that promotes wound repair. Developmental cell *31*, 48-60.